



Article

# Technetium Encapsulation by A Nanoporous Complex Oxide $12\text{CaO}\cdot 7\text{Al}_2\text{O}_3$ (C12A7)

Navaratnarajah Kuganathan <sup>1,2,\*</sup> and Alexander Chroneos <sup>1,2</sup>

<sup>1</sup> Department of Materials, Imperial College London, London SW7 2AZ, UK; alexander.chroneos@imperial.ac.uk

<sup>2</sup> Faculty of Engineering, Environment and Computing, Coventry University, Priory Street, Coventry CV1 5FB, UK

\* Correspondence: n.kuganathan@imperial.ac.uk or ad0636@coventry.ac.uk

Received: 13 May 2019; Accepted: 29 May 2019; Published: 30 May 2019



**Abstract:** Technetium ( $^{99}\text{Tc}$ ) is an important long-lived radionuclide released from various activities including nuclear waste processing, nuclear accidents and atmospheric nuclear weapon testing. The removal of  $^{99}\text{Tc}$  from the environment is a challenging task, and chemical capture by stable ceramic host systems is an efficient strategy to minimise the hazard. Here we use density functional theory with dispersion correction (DFT+D) to examine the capability of the porous inorganic framework material C12A7 that can be used as a filter material in different places such as industries and nuclear power stations to encapsulate Tc in the form of atoms and dimers. The present study shows that both the stoichiometric and electride forms of C12A7 strongly encapsulate a single Tc atom. The electride form exhibits a significant enhancement in the encapsulation. Although the second Tc encapsulation is also energetically favourable in both forms, the two Tc atoms prefer to aggregate, forming a dimer.

**Keywords:** technetium; DFT; encapsulation; C12A7; electride

## 1. Introduction

Long-lived Technetium ( $^{99}\text{Tc}$ ) is a dominant radionuclide which is mainly introduced into the environment due to human activities such as nuclear weapon testing, nuclear spent fuel reprocessing and radio-pharmaceutical activities [1–4]. Importantly, technetium has radioactivity with a long half-life ( $2.1 \times 10^5$  years), and there is a health risk when it enters the human body [4,5]. Thus, the effective capture of Tc from the environment is of great interest.

There has been an extensive search for candidate host materials to trap radionuclides [6–9]. The requirements imposed on host materials are high thermodynamical, chemical, and mechanical stability. A number of host materials including zeolites, buckyballs ( $\text{C}_{60}$ ), carbon nanotubes and metal organic frameworks have been studied extensively [10–14]. The buckyball structured fullerenes have been recently considered as candidate host materials for the encapsulation or trapping of many species, including radionuclides, as they have open structures with very high mechanical stability at high temperatures and are chemically inert [15–20]. Saha et al. [21] applied a recoil implantation technique to encapsulate a variety of radio isotopes for future application in radioactive endohedral fullerenes. Endohedral encapsulation of single Tc atoms and Tc clusters was studied theoretically to predict the structures and magnetic properties of the resultant complexes by Weck et al. [22]. Silica zeolite was effectively used by Pham et al. [23] to capture radioactive iodine, which directly affects the human metabolic system. Peng et al. [24] proposed a new strategy to trap radioactive barium and other nuclides using a metal organic framework. The search for cheaper and “greener” alternative stable host materials continues.

$12\text{CaO}\cdot 7\text{Al}_2\text{O}_3$  (C12A7) is a complex inorganic oxide exhibiting high thermal and chemical stability [25] (refer to Figure 1). The stability of this material under harsh conditions and its powder form are beneficial to preparing filters in experiments and capturing Tc efficiently. Its unusual crystal structure consists of 12 nano cages per unit cell, making this material promising for accommodating a large number of foreign species such as atoms or small molecules [25,26]. Additionally, its constituent elements are non-toxic and highly abundant. The cubic unit cell of stoichiometric C12A7 is represented by the formula  $[\text{Ca}_{24}\text{Al}_{28}\text{O}_{64}]^{4+}\cdot 2\text{O}^{2-}$  (C12A7: $\text{O}^{2-}$ ) [25,26], in which the cation  $[\text{Ca}_{24}\text{Al}_{28}\text{O}_{64}]^{4+}$  makes up the framework of 12 equivalent cages, each having a mean effective charge of  $1/3 |e|$  and connected to eight neighbouring cages via  $\sim 0.1$  nm wide openings. The two  $\text{O}^{2-}$  ions compensate the positive charge of the framework. They occupy one in six cages and are often referred to as extra-framework or “free” anions. The extra-framework  $\text{O}^{2-}$  ions are relatively loosely bound to the framework and can be either removed or replaced with other species, such as  $\text{H}^-$ ,  $\text{OH}^-$ ,  $\text{Au}^-$ ,  $\text{NH}_2^-$ ,  $\text{F}^-$ , and others [27–34]. Complete replacement of two extra-framework  $\text{O}^{2-}$  ions can also occur with four electrons by effective reduction methods. This form of C12A7 is regarded as an electride, i.e., a material in which electrons act as anions, and is denoted as C12A7: $e^-$  [35,36].

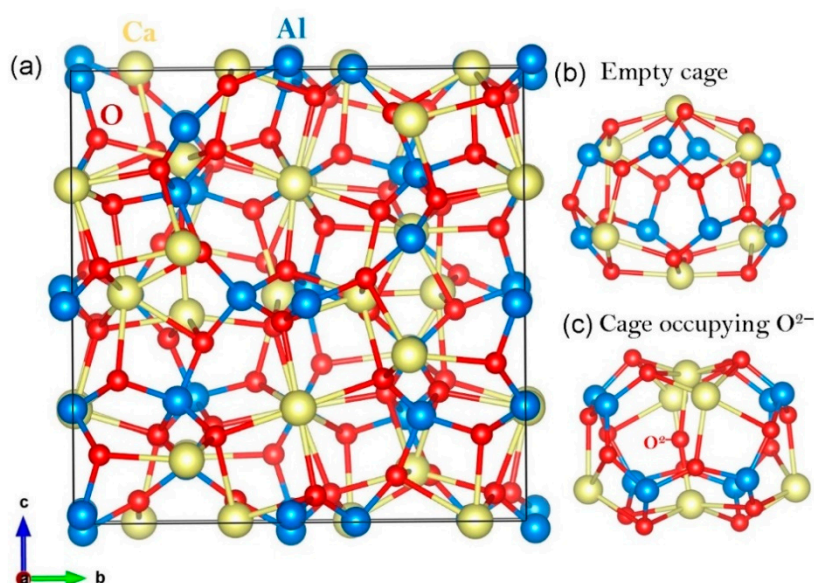


**Figure 1.** (a) Crystal structure of  $[\text{Ca}_{24}\text{Al}_{28}\text{O}_{64}]^{4+}$  containing twelve empty cages; (b) and (c) optimised structures of an empty cage and a cage with an extra-framework  $\text{O}^{2-}$  ion in C12A7: $\text{O}^{2-}$ , respectively.

In the present study, density functional theory with dispersion correction (DFT+D) is used to examine the thermodynamic stability of gas-phase Tc atoms and a Tc dimer encapsulated within C12A7 by calculating the encapsulation energies, Bader charges on encapsulated atoms, density of states (DOS) plots and charge density plots. This study can provide useful information about the practical applicability of this material in filters used in many places, including nuclear reprocessing plants and pharmaceutical industries. Furthermore, the application of this material can be extended to the efficient capture of Tc released into the environment during unexpected nuclear accidents. DFT calculations provide valuable information on equilibrium structures, charge transfer and electronic properties.

## 2. Computational Methods

We used DFT together with spin polarisation as implemented in the Vienna Ab initio Simulation Package (VASP) code [37] to calculate the electronic structures of Tc atoms and a Tc dimer encapsulated within C12A7 nanopores. The DFT method is powerful tool to model periodic systems (e.g., C12A7) and provide accurate information on structures, electronic structures, charge transfer and weak intermolecular forces. In previous studies, we used DFT methods to model a variety

of species encapsulated in different host materials [38–51]. There were 118 and 116 atoms present in the stoichiometric and electrified forms of the cubic supercell, respectively. Generalised gradient approximation (GGA) parameterised by Perdew, Burke, and Ernzerhof (PBE) was used to describe the exchange–correlation term [52]. A plane wave basis set of 500 eV and a  $2 \times 2 \times 2$  Monkhorst–Pack  $k$ -point mesh [53] were used. This combination was used in previous studies, and further increase in the cut-off energy or  $k$  resulted in negligible change in the total energy [32]. For bulk Tc, an  $8 \times 8 \times 6$  Monkhorst–Pack  $k$ -point mesh was used. Geometry optimisations were carried out using a conjugate gradient algorithm [54]. Forces on the atoms were calculated using the Hellman–Feynman theorem; the Pulay corrections were smaller than  $0.001 \text{ eV}/\text{\AA}$ , and the atomic stress tensor values were less than  $0.002 \text{ GPa}$ . The encapsulation energy for a single Tc atom inside an empty cage of the electrified form of C12A7 is defined by the following equation:

$$E_{\text{Enc}} = E(\text{Tc:C12A7:e}^-) - E(\text{C12A7:e}^-) - E(\text{Tc}) \quad (1)$$

where  $E(\text{C12A7:e}^-)$  is the total energy for bulk C12A7:e<sup>−</sup>,  $E(\text{Tc:C12A7:e}^-)$  is the total energy of the Tc atom occupying the cages, and  $E(\text{Tc})$  is the total energy of an isolated Tc atom (the reference state).

Here, semi-empirical dispersion corrections were included using the pair-wise force field as implemented by Grimme et al. [55] [DFT-D3 (zero)] in VASP.

### 3. Results

#### 3.1. Structural Modelling of Bulk Tc and C12A7

First, the validity of the pseudopotentials and basis sets was examined by performing energy minimisation calculations on bulk Tc and bulk C12A7 and comparing the equilibrium lattice constants with corresponding experimental values.

Hexagonal bulk Tc (space group P63/mmc) was optimised under constant pressure to validate the pseudopotential and basis set used for Tc. The calculated lattice constants are in good agreement with the experimental values reported by Lam et al. [56]. Table 1 reports the comparison of the lattice constant values obtained by the experiment and this study.

**Table 1.** Comparison between the experimental and calculated structural parameters of hexagonal (P63/mmc) Tc.

Parameter	Calcd	Exptl [56]	\Delta  (%)
a = b (Å)	2.723	2.743	0.73
c (Å)	4.378	4.400	0.50
$\alpha = \beta$	90.00	90.00	0.00
$\gamma$ (°)	120.0	120.0	0.00
V (Å <sup>3</sup> )	28.26	28.67	1.43

The cubic unit cell of stoichiometric C12A7 (space group  $(\bar{I}43d)$ ) has a lattice constant of  $11.99 \text{ \AA}$  [26]. The experimental structure of C12A7:O<sup>2−</sup> was optimised to validate the pseudopotentials and basis sets used for Ca, Al and O. There is a good reproduction between the calculated and experimental lattice constants as observed in our previous study [32] (refer to Table 2). There is a small distortion in the cubic symmetry due to the attraction between the extra-framework O<sup>2−</sup> and the cage wall Ca<sup>2+</sup> ions introducing a small perturbation in the lattice parameters (refer to Figure 1). Nevertheless, this distortion is small and can be deemed acceptable.

**Table 2.** Comparison between the experimental and calculated structural parameters of cubic ( $\bar{I}43d$ )  $C_{12}A_7O^{2-}$ .

Parameter	Calcd	Exptl [26]	$ \Delta (\%)$
a (Å)	12.04	11.99	0.42
b (Å)	12.01	11.99	0.17
c (Å)	12.01	11.99	0.17
$\alpha$ (°)	90.02	90.0	0.02
$\beta$ (°)	89.95	90.0	0.06
$\gamma$ (°)	89.93	90.0	0.08
V (Å <sup>3</sup> )	1738.66	1727.38	0.65

### 3.2. Encapsulation of Single Tc Atoms in A Cage of $C_{12}A_7O^{2-}$

The thermodynamic stability of a single Tc atom encapsulated within one of the ten empty cages in stoichiometric  $C_{12}A_7$  was examined. Figure 2 shows the relaxed structure and the cage containing the Tc atom. Tc occupies a position slightly off centre in the cage, forming strong Tc–O bonds with bond distances of 2.33 Å and 2.54 Å. Nevertheless, the Tc–Ca and Tc–Al distances are relatively long (Tc–Ca: 2.87 Å and 3.14 Å, Tc–Al: 2.97 Å) due to the repulsion between cations. This is reflected in the Ca–Ca cage pole distance (5.86 Å). There is a 0.2 Å elongation in the Ca–Ca cage pole distance compared to that of the empty cage (refer to Figure 2). The encapsulation energy is  $-2.24$  eV, suggesting that a gaseous Tc atom is more stable inside the cage than its isolated form. The Bader charge analysis [57] result on the Tc is +0.13. This small Bader charge is due to the net interactions between Tc and cations and anions. The overall structure of the lattice was not significantly affected by the encapsulation of a single Tc. Figure 2c,d show the DOS plots for  $C_{12}A_7O^{2-}$  and Tc encapsulated within  $C_{12}A_7O^{2-}$  (Tc:  $C_{12}A_7O^{2-}$ ), respectively.  $C_{12}A_7O^{2-}$  is an insulator with a wide band gap. Encapsulation of Tc introduces gap states closer to the Fermi level, and the resultant complex is still an insulator.

Thereafter, we considered an additional Tc atom in a cage adjacent to the cage with a pre-existing Tc. The relaxed cages are shown in Figure 3a. The Ca–Ca cage pole distances were calculated to be 5.85 and 6.00 Å, again showing the repulsion between Tc and cage pole  $Ca^{2+}$  ions. Tc atoms are displaced slightly away from the centre of the cages and interact with cage wall ions. The calculated Tc–O bond distances were 2.24 Å and 2.74 Å. The encapsulation energy for the second Tc atom into the Tc: $C_{12}A_7O^{2-}$  is  $-2.36$  eV, suggesting that further incorporation of Tc into the empty cages is energetically feasible. The second incorporation energy is slightly more negative (by 0.12 eV) than the first incorporation energy. This is due to the small expansion of volume introduced by the previous geometry optimisation for Tc: $C_{12}A_7O^{2-}$ . The Bader analysis shows that both Tc atoms exhibit a +0.13 charge. The DOS plot is shown in Figure 3b. Additional states are introduced in the band gap by the second Tc atom. The introduction of Tc atoms into the cages leaves the composite magnetic according to the DOS plot as the spin-up and spin-down states are not equal, particularly in the band gap region.

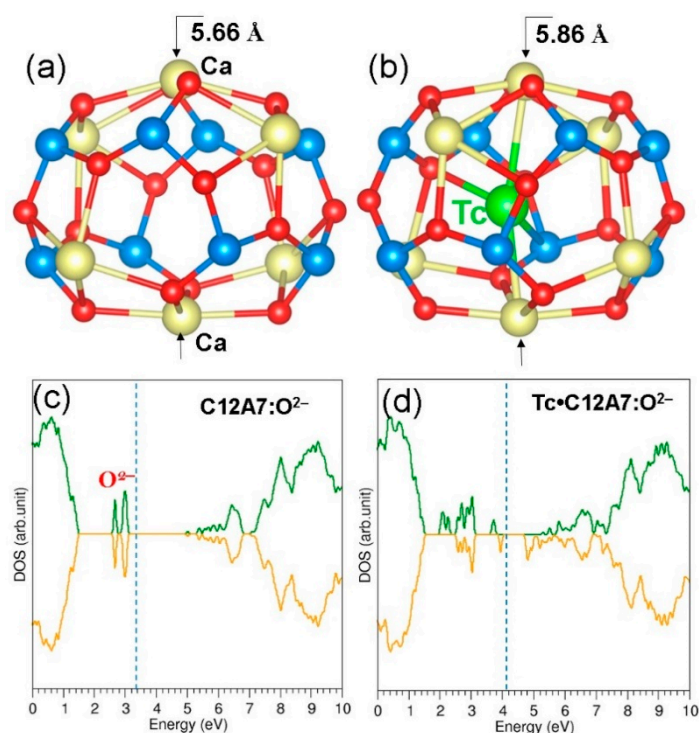


**Figure 2.** (a) and (b) Optimised structures of an empty cage and a cage containing a Tc atom, respectively, showing the Ca–Ca cage pole distance; (c) and (d) density of states (DOS) plots calculated for C12A7:O<sup>2-</sup> and Tc:C12A7:O<sup>2-</sup>, respectively. The vertical blue dotted lines correspond to the Fermi energy.

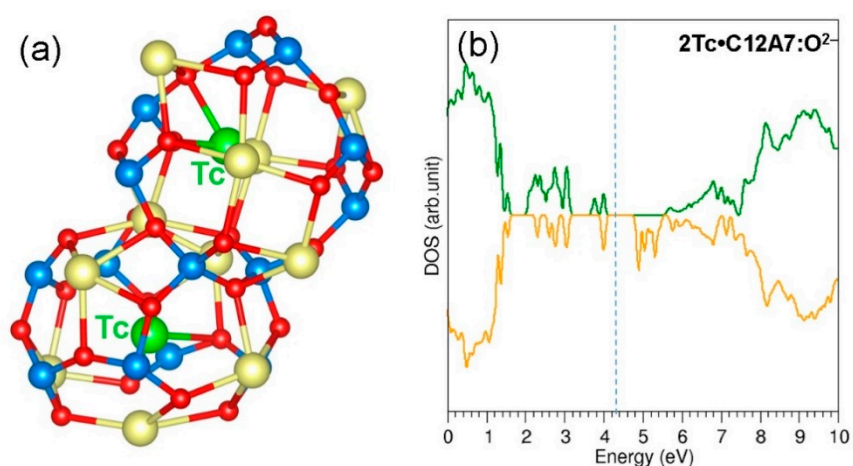


**Figure 3.** (a) Relaxed cages containing two Tc atoms in C12A7:O<sup>2-</sup> and (b) DOS plot calculated for 2Tc:C12A7:O<sup>2-</sup>.

### 3.3. Encapsulation of Single Tc Atoms in C12A7:e<sup>-</sup>

The electride form of C12A7 was next considered for the encapsulation of a single Tc atom. Figure 4d shows the optimised structure of the cage with encapsulated Tc. In order to compare the deformation, the optimised structure of an empty cage in C12A7:e<sup>-</sup> is also shown in Figure 4a. The encapsulated Tc atom occupies a space between two Ca<sup>2+</sup> ions in the cage wall (center of the cage). This is due to the strong attraction between Tc and the positively charged cage wall Ca<sup>2+</sup> ions. This is further supported by the Bader charge on the Tc (−0.90 |e|). The negative charge on the Tc atom was transferred from the extra framework electrons available in the electride form of C12A7. The cage wall distance (refer to Figure 4d) is 5.53 Å. This is shorter by 0.17 Å than that calculated for an empty cage (refer to Figure 4a). This is due to the electrostatic attraction between the negatively

charged Tc and positively charged cage wall  $\text{Ca}^{2+}$  ions. The encapsulation energy was calculated to be  $-3.56$  eV. This is more negative by  $\sim 1.30$  eV than that calculated for single Tc encapsulation within  $\text{C12A7:O}^{2-}$ . This significant enhancement in the encapsulation energy is due to the delocalised electrons in  $\text{C12A7:e}^-$ . These electrons enabled Tc to gain a small number of electrons to form a negative ion which introduces an attractive interaction with cage wall  $\text{Ca}^{2+}$  ions. Figure 4b,e show the DOS plots for  $\text{C12A7:e}^-$  and  $\text{Tc:C12A7:e}^-$ , respectively.  $\text{C12A7:e}^-$  is metallic. The encapsulation of Tc reduces the number of electrons in  $\text{C12A7:e}^-$  and forms a  $\text{Tc}^-$  ion. The resultant complex is still metallic (refer to Figure 4e) as there are three electrons available in the unit cell of  $\text{C12A7:e}^-$ . In order to confirm the electron transfer from  $\text{C12A7:e}^-$  to Tc, we plotted constant charge density plots for both  $\text{C12A7:e}^-$  and  $\text{Tc:C12A7:e}^-$  (refer to Figure 4c,f). There is a reduction in the electron charge density in the empty cages of  $\text{Tc:C12A7:e}^-$ , and there is an electron cloud localised on the Tc atom, ensuring the electron transfer.

The second Tc atom was next encapsulated within a cage adjacent to the cage with a pre-existing Tc. The relaxed structure of the cages containing Tc atoms is shown in Figure 5a. Both Tc atoms occupy the centre of the cages. The cage pole distances are  $5.52$  Å and  $5.63$  Å, showing the attractive interaction between Tc and  $\text{Ca}^{2+}$  ions. The Bader charges on the Tc atoms are  $-0.81$  |e| and  $-0.93$  |e|. This indicates that the second Tc atom also gains  $\sim 1$  electron from the extra-framework electrons. There is a reduction in the encapsulation energy ( $-2.53$  eV) for the second Tc. This is due to the lesser number of electrons (three electrons) available in the  $\text{Tc:C12A7:e}^-$  complex. Figure 5b shows the DOS plot calculated for  $2\text{Tc:C12A7:e}^-$ . The resultant complex is metallic as there are two extra-framework electrons available in the lattice. The charge density plot is shown in Figure 5c. Both Tc atoms are surrounded by electrons. The rest of the electrons are localised closer to the cages occupied by the Tc atoms.

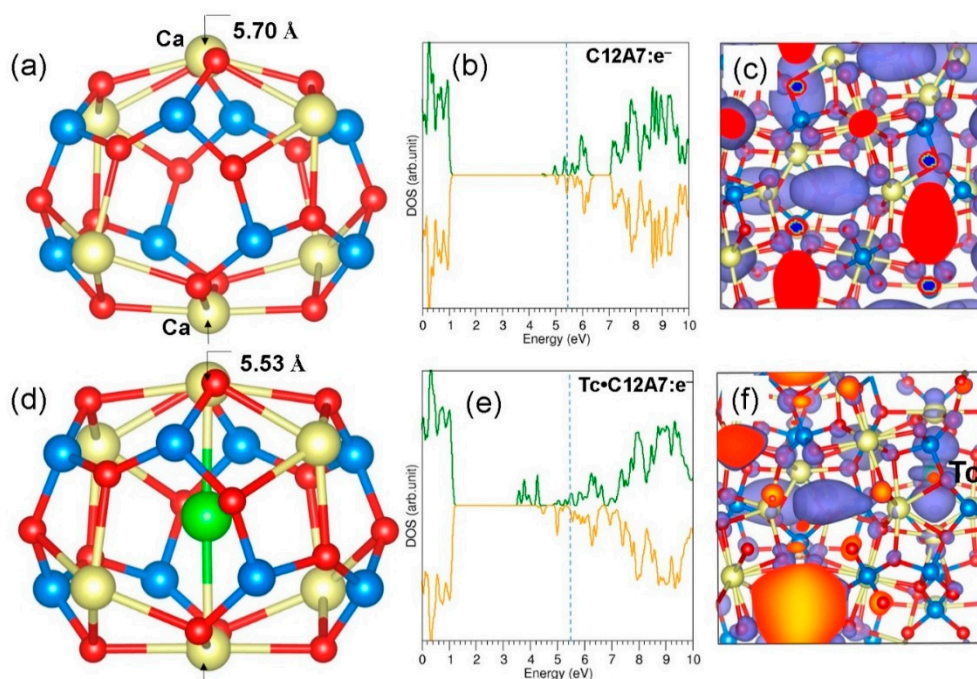


**Figure 4.** (a) Relaxed empty cage showing the Ca–Ca pole distance in  $\text{C12A7:e}^-$ ; (b) DOS plot calculated for  $\text{C12A7:e}^-$ ; (c) charge density plot showing four electrons delocalised in  $\text{C12A7:e}^-$ ; (d) relaxed cage containing Tc; (e) DOS plot calculated for  $\text{Tc:C12A7:e}^-$ ; and (f) charge density plot showing the localisation of some electrons on the Tc atom.

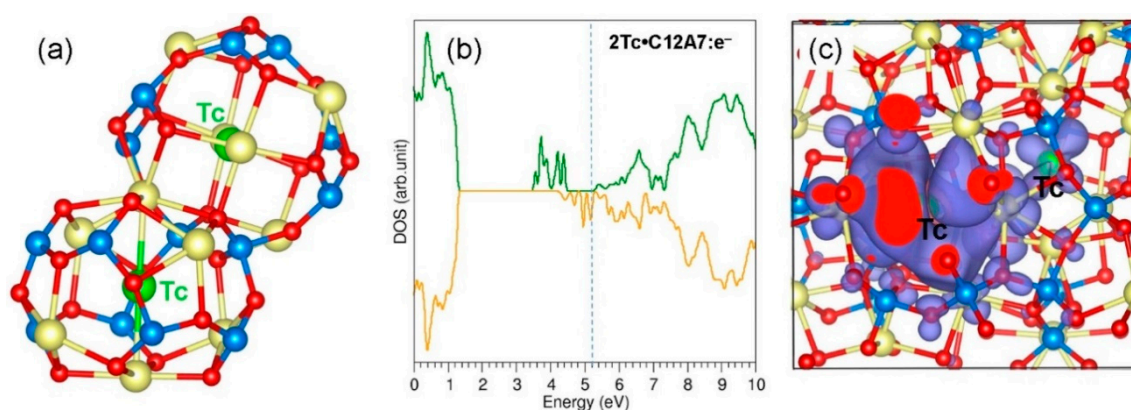


**Figure 5.** (a) Relaxed structure of two Tc atoms encapsulated in two adjacent cages in  $C12A7:e^-$ ; (b) DOS plot calculated for  $2Tc: C12A7:e^-$ ; and (c) charge density plot showing the distribution of electrons in the lattice.

### 3.4. Stability of a Tc Dimer in $C12A7:O^{2-}$

Here we examine the formation of a Tc dimer in an empty cage of  $C12A7:O^{2-}$ . The relaxed structure of the Tc dimer encapsulated within an empty cage is shown in Figure 6a. The Tc–Tc bond distance is 1.95 Å. This ensures the formation of a dimer. The encapsulation energy of the dimer was calculated according to three different processes (refer to Table 3). In the first process, two gas-phase Tc atoms are encapsulated by  $C12A7:O^{2-}$  to form a dimer. The encapsulation energy is  $-3.78$  eV. The formation of the Tc dimer was considered to be due to the reaction between a single Tc atom and  $Tc:C12A7:O^{2-}$  in the second process. In this process, the encapsulation energy is  $-2.65$  eV. The lower encapsulation energy is due to the energy required to reorient the pre-existing Tc to form the dimer. In the third process, the encapsulation was considered to be of a gas-phase Tc dimer. The encapsulation energy ( $-1.16$  eV) is still exoergic but is lower than the values calculated in the other processes. This is due to the longer Tc–Tc bond distance by 0.11 Å than that calculated for the gas-phase Tc dimer. The total energy difference between a Tc dimer in an empty cage and two Tc atoms in two adjacent  $C12A7:O^{2-}$  cages was calculated. A Tc dimer in an empty cage is more stable (by 2.96 eV) than the two isolated Tc atoms occupying adjacent cages. The Bader charges on the Tc atoms are  $-0.44$  and  $+0.33$ , indicating that the dimer is polarised. The relaxed structure of the cage is slightly distorted due to the attractive (between the positively charged Tc and cage wall  $O^{2-}$  ions) and repulsive (negatively charged Tc and cage wall  $O^{2-}$  ions) forces.

**Table 3.** Encapsulation energy and Bader charge calculated for the formation of a Tc dimer inside  $C12A7:O^{2-}$ .

Reaction	Encapsulation Energy (eV/atom) with Respect to Tc Atom	Bader Charge  e  on Tc
$Tc + Tc + C12A7:O^{2-} \rightarrow Tc_2: C12A7:O^{2-}$	$-3.78$	
$Tc + Tc: C12A7:O^{2-} \rightarrow Tc_2: C12A7:O^{2-}$	$-2.65$	
	with respect to Tc dimer (eV/atom)	$+0.33, -0.44$
$Tc_2 + C12A7:O^{2-} \rightarrow Tc_2: C12A7:O^{2-}$	$-1.16$	

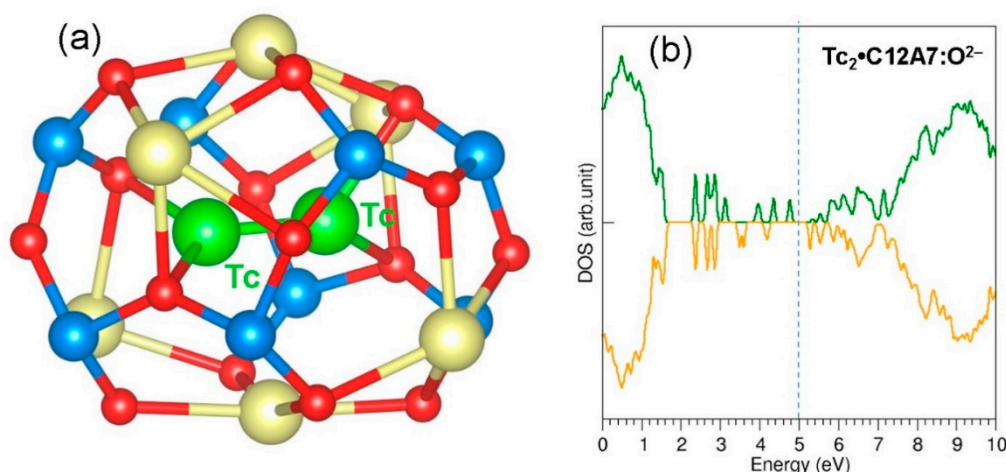


**Figure 6.** (a) Relaxed cage structure showing the accommodation of the Tc dimer in  $C12A7:O^{2-}$  and (b) DOS plot calculated for  $Tc_2: C12A7:O^{2-}$ .

### 3.5. Stability of a Tc Dimer in $C12A7:e^-$

Finally, we considered the stability of a Tc dimer in an empty cage in  $C12A7:e^-$ . The optimised structure of the dimer inside the cage is shown in Figure 7a. The dimer distance is 2.04 Å, slightly longer (by 0.2 Å) than the gas-phase dimer distance. The elongation is due to the repulsion between the two negatively charged Tc atoms. The Bader charges on the Tc atoms are  $-0.52 |e|$  and  $-0.38 |e|$ , suggesting that the dimer is reduced to form a  $(Tc_2)^-$  ion (refer to Table 4). The Tc–O distances (2.52 Å, 2.87 Å, and 2.98 Å) are longer than the values calculated in  $C12A7:O^{2-}$  as there is a repulsion between the Tc and cage wall  $O^{2-}$  ions. The encapsulation energy for dimer formation from two Tc gas-phase atoms is  $-3.93$  eV (refer to Table 4). The encapsulation of a dimer via this route is more easily facilitated (by 0.16 eV) than that observed in  $C12A7:O^{2-}$ . The encapsulation energy for a single gas-phase Tc atom to combine with  $Tc:C12A7:e^-$  to form a dimer is  $-2.15$  eV. As discussed earlier, this is due to the energy required to reorient the pre-existing Tc atom in the cage. There is a reduction in the encapsulation energy by 0.50 eV compared to the similar process in  $C12A7:O^{2-}$ . This is due to the stronger attraction between the negatively charged Tc atom and the cage wall  $Ca^{2+}$  ions. The dimer configuration is 1.77 eV more stable than the two isolated Tc atoms occupying adjacent cages. The encapsulation energy calculated using the dimer as a reference is  $-1.31$  eV, slightly (by 0.15 eV) more favourable than that observed in  $C12A7:O^{2-}$ .

**Table 4.** Encapsulation energy and Bader charge calculated for the formation of the Tc dimer inside  $C12A7:e^-$ .

Reaction	Encapsulation Energy (eV/atom) with Respect to Tc Atom	Bader Charge $ e $ on Tc
$Tc + Tc + C12A7:e^- \rightarrow Tc_2: C12A7:e^-$	$-3.93$	
$Tc + Tc: C12A7:e^- \rightarrow Tc_2: C12A7:e^-$	$-2.15$	
	with respect to Tc dimer (eV/atom)	$-0.38, -0.51$
$Tc_2 + C12A7:e^- \rightarrow Tc_2: C12A7:e^-$	$-1.31$	

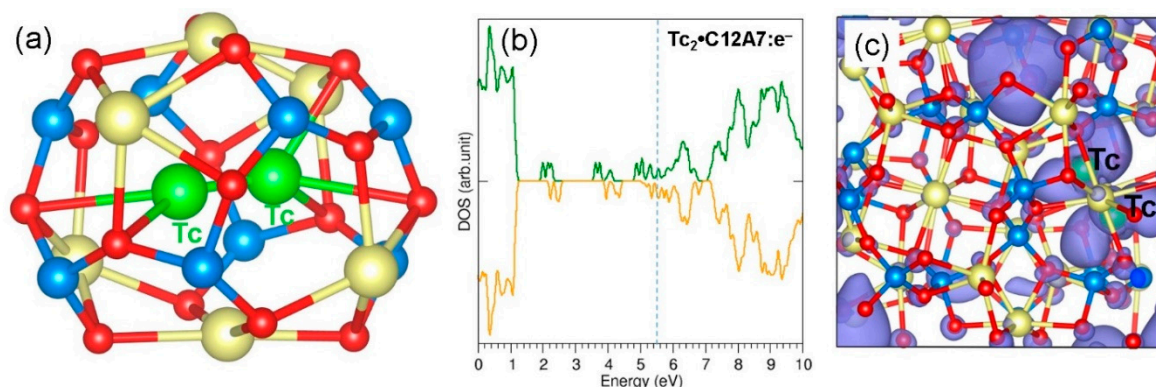


**Figure 7.** (a) Relaxed cage structure showing the Tc dimer in C12A7:e<sup>-</sup>; (b) DOS plot calculated for Tc<sub>2</sub>:C12A7:e<sup>-</sup>; and (c) charge density plot associated with the electron distribution.

#### 4. Conclusions

We used DFT with dispersion correction to study the encapsulation of gas-phase Tc atoms and dimers into the stoichiometric and electroneutral forms of C12A7. Both forms of C12A7 strongly encapsulate a single Tc atom, and their encapsulation energies are  $-2.26$  eV and  $-3.56$  eV, respectively. These exoergic encapsulation energies suggest that a single Tc atom is more favourable inside the cages of both forms of C12A7 than its gas phase. There is a significant enhancement in the encapsulation energy for C12A7:e<sup>-</sup> due to the extra-framework electrons being reflected in the Bader charges. The second encapsulation is also exoergic in both cases, suggesting that this material has the ability to encapsulate multiple atoms. The encapsulation energies for the formation of a dimer via encapsulation of two gas-phase Tc atoms in C12A7:O<sup>2-</sup> and C12A7:e<sup>-</sup> are  $-3.78$  eV and  $-3.93$  eV, respectively. The similar encapsulation of a dimer as a reference is less favoured than the former. Our study further suggests that two isolated Tc atoms in adjacent cages would prefer to form a dimer in both C12A7:O<sup>2-</sup> and C12A7:e<sup>-</sup>. The maximum number of Tc atoms with exoergic encapsulation should be our interest in future work.

**Author Contributions:** Computation, N.K.; Writing, N.K.; Analysis and Editing, A.C.

**Funding:** This research received no external funding.

**Acknowledgments:** We acknowledge Imperial College for providing high-performance computing facilities.

**Conflicts of Interest:** The authors declare no conflict of interest.

#### References

1. Beals, D.M. Determination of technetium-99 in aqueous samples by isotope dilution inductively coupled plasma-mass spectrometry. *J. Radioanal. Nucl. Chem.* **1996**, *204*, 253–263. [[CrossRef](#)]
2. Garcia-Leon, M. <sup>99</sup>Tc in the environment: Sources, distribution and methods. *J. Nucl. Radiochem. Sci.* **2005**, *6*, 253–259.
3. Schulte, E.H.; Scoppa, P. Sources and behavior of technetium in the environment. *Sci. Total Environ.* **1987**, *64*, 163–179. [[CrossRef](#)]
4. Shi, K.; Hou, X.; Roos, P.; Wu, W. Determination of technetium-99 in environmental samples: A review. *Anal. Chim. Acta* **2012**, *709*, 1–20. [[CrossRef](#)]
5. Berlyn, G.P.; Dhillon, S.S.; Koslow, E.E. Technetium: A toxic waste product of the nuclear fuel cycle: Effects on soybean growth and development. *Environ. Manag.* **1980**, *4*, 149–156. [[CrossRef](#)]
6. McMaster, S.A.; Ram, R.; Faris, N.; Pownceby, M.I. Radionuclide disposal using the pyrochlore super group of minerals as a host matrix—A review. *J. Hazard. Mater.* **2018**, *360*, 257–269. [[CrossRef](#)]
7. Higgo, J.J.W. Clay as a barrier to radionuclide migration. *Prog. Nucl. Energy* **1987**, *19*, 173–207. [[CrossRef](#)]

8. Sun, Q.; Zhu, L.; Aguila, B.; Thallapally, P.K.; Xu, C.; Chen, J.; Wang, S.; Rogers, D.; Ma, S. Optimizing radionuclide sequestration in anion nanotraps with record pertechnetate sorption. *Nat. Commun.* **2019**, *10*, 1646. [[CrossRef](#)]
9. Claverie, M.; Garcia, J.; Prevost, T.; Brendlé, J.; Limousy, L. Inorganic and Hybrid (Organic–Inorganic) Lamellar Materials for Heavy Metals and Radionuclides Capture in Energy Wastes Management—A Review. *Materials* **2019**, *12*, 1399. [[CrossRef](#)]
10. Shilina, A.S.; Bakhtin, V.D.; Burukhin, S.B.; Askhadullin, S.R. Sorption of cations of heavy metals and radionuclides from the aqueous media by new synthetic zeolite-like sorbent. *Nucl. Energy Technol.* **2017**, *3*, 249–254. [[CrossRef](#)]
11. Yang, H.; Luo, M.; Luo, L.; Wang, H.; Hu, D.; Lin, J.; Wang, X.; Wang, Y.; Wang, S.; Bu, X.; et al. Highly Selective and Rapid Uptake of Radionuclide Cesium Based on Robust Zeolitic Chalcogenide via Stepwise Ion-Exchange Strategy. *Chem. Mater.* **2016**, *28*, 8774–8780. [[CrossRef](#)]
12. Gadd, G.E.; Evans, P.J.; Hurwood, D.J.; Moricca, S.; McOrist, G.; Wall, T.; Elcombe, M.; Prasad, P. Endohedral Formation from Neutron Activation of Interstitial Rare Gas C<sub>60</sub> Fullerides. *Fuller. Sci. Technol.* **1997**, *5*, 871–902. [[CrossRef](#)]
13. Ohtsuki, T.; Ohno, K. Radiochemical approaches for formation of endohedral fullerenes and MD simulation. *Sci. Technol. Adv. Mater.* **2004**, *5*, 621–624. [[CrossRef](#)]
14. Belloni, F.; Kütahyalı, C.; Rondinella, V.V.; Carbol, P.; Wiss, T.; Mangione, A. Can carbon nanotubes play a role in the field of nuclear waste management? *Environ. Sci. Technol.* **2009**, *43*, 1250–1255. [[CrossRef](#)] [[PubMed](#)]
15. Diederich, F.; Whetten, R.L. Beyond C<sub>60</sub>: The higher fullerenes. *Acc. Chem. Res.* **1992**, *25*, 119–126. [[CrossRef](#)]
16. Kuganathan, N.; Arya, A.K.; Rushton, M.J.D.; Grimes, R.W. Trapping of volatile fission products by C<sub>60</sub>. *Carbon* **2018**, *132*, 477–485. [[CrossRef](#)]
17. Kuganathan, N.; Selvanantharajah, N.; Iyngaran, P.; Abiman, P.; Chroneos, A. Cadmium trapping by C<sub>60</sub> and B-, Si-, and N-doped C<sub>60</sub>. *J. Appl. Phys.* **2019**, *125*, 054302. [[CrossRef](#)]
18. Kuganathan, N.; Green, J.C.; Himmel, H.-J. Dinitrogen fixation and activation by Ti and Zr atoms, clusters and complexes. *New J. Chem.* **2006**, *30*, 1253–1262. [[CrossRef](#)]
19. Srivastava, A.K.; Pandey, S.K.; Misra, N. Encapsulation of lawrencium into C<sub>60</sub> fullerene: Lr@C<sub>60</sub> versus Li@C<sub>60</sub>. *Mater. Chem. Phys.* **2016**, *177*, 437–441. [[CrossRef](#)]
20. Kikuchi, K.; Kobayashi, K.; Sueki, K.; Suzuki, S.; Nakahara, H.; Achiba, Y.; Tomura, K.; Katada, M. Encapsulation of Radioactive 159Gd and 161Tb Atoms in Fullerene Cages. *J. Am. Chem. Soc.* **1994**, *116*, 9775–9776. [[CrossRef](#)]
21. Saha, S.K.; Chowdhury, D.P.; Das, S.K.; Guin, R. Encapsulation of radioactive isotopes into C<sub>60</sub> fullerene cage by recoil implantation technique. *Nucl. Instrum. Methods Phys. Res. Sect. B* **2006**, *243*, 277–281. [[CrossRef](#)]
22. Weck, P.F.; Kim, E.; Czerwinski, K.R.; Tománek, D. Structural and magnetic properties of Tc<sub>n</sub>@C<sub>60</sub> endohedral metallofullerenes: First-principles predictions. *Phys. Rev. B* **2010**, *81*, 125448. [[CrossRef](#)]
23. Pham, T.C.T.; Docao, S.; Hwang, I.C.; Song, M.K.; Choi, D.Y.; Moon, D.; Oleynikov, P.; Yoon, K.B. Capture of iodine and organic iodides using silica zeolites and the semiconductor behaviour of iodine in a silica zeolite. *Energy Environ. Sci.* **2016**, *9*, 1050–1062. [[CrossRef](#)]
24. Peng, Y.; Huang, H.; Liu, D.; Zhong, C. Radioactive Barium Ion Trap Based on Metal–Organic Framework for Efficient and Irreversible Removal of Barium from Nuclear Wastewater. *ACS Appl. Mater. Interfaces* **2016**, *8*, 8527–8535. [[CrossRef](#)]
25. Watauchi, S.; Tanaka, I.; Hayashi, K.; Hirano, M.; Hosono, H. Crystal growth of Ca<sub>12</sub>Al<sub>14</sub>O<sub>33</sub> by the floating zone method. *J. Cryst. Growth* **2002**, *237–239*, 801–805. [[CrossRef](#)]
26. Imlach, J.A.; Dent Glasser, L.S.; Glasser, F.P. Excess oxygen and the stability of “12CaO·7Al<sub>2</sub>O<sub>3</sub>”. *Cem. Concr. Res.* **1971**, *1*, 57–61. [[CrossRef](#)]
27. Hayashi, K.; Hirano, M.; Hosono, H. Thermodynamics and Kinetics of Hydroxide Ion Formation in 12CaO·7Al<sub>2</sub>O<sub>3</sub>. *J. Phys. Chem. B* **2005**, *109*, 11900–11906. [[CrossRef](#)]
28. Miyakawa, M.; Kamioka, H.; Hirano, M.; Kamiya, T.; Sushko, P.V.; Shluger, A.L.; Matsunami, N.; Hosono, H. Photoluminescence from Au ion-implanted nanoporous single-crystal. 12CaO·7Al<sub>2</sub>O<sub>3</sub>. *Phys. Rev. B* **2006**, *73*, 205108. [[CrossRef](#)]
29. Kuganathan, N.; Hosono, H.; Shluger, A.L.; Sushko, P.V. Enhanced N<sub>2</sub> Dissociation on Ru-Loaded Inorganic Electride. *J. Am. Chem. Soc.* **2014**, *136*, 2216–2219. [[CrossRef](#)]

30. Kitano, M.; Kanbara, S.; Inoue, Y.; Kuganathan, N.; Sushko, P.V.; Yokoyama, T.; Hara, M.; Hosono, H. Electride support boosts nitrogen dissociation over ruthenium catalyst and shifts the bottleneck in ammonia synthesis. *Nat. Commun.* **2015**, *6*, 6731. [[CrossRef](#)]
31. Toda, Y.; Hirayama, H.; Kuganathan, N.; Torrisi, A.; Sushko, P.V.; Hosono, H. Activation and splitting of carbon dioxide on the surface of an inorganic electride material. *Nat. Commun.* **2013**, *4*, 2378. [[CrossRef](#)]
32. Kuganathan, N.; Grimes, R.W.; Chroneos, A. Encapsulation of heavy metals by a nanoporous complex oxide  $12\text{CaO}\cdot 7\text{Al}_2\text{O}_3$ . *J. Appl. Phys.* **2019**, *125*, 165103. [[CrossRef](#)]
33. Song, C.; Sun, J.; Qiu, S.; Yuan, L.; Tu, J.; Torimoto, Y.; Sadakata, M.; Li, Q. Atomic Fluorine Anion Storage Emission Material  $\text{C}_{12}\text{A}_7\text{-F}$ —and Etching of Si and  $\text{SiO}_2$  by Atomic Fluorine Anions. *Chem. Mater.* **2008**, *20*, 3473–3479. [[CrossRef](#)]
34. Hayashi, F.; Tomota, Y.; Kitano, M.; Toda, Y.; Yokoyama, T.; Hosono, H.  $\text{NH}_2^-$  Dianion Entrapped in a Nanoporous  $12\text{CaO}\cdot 7\text{Al}_2\text{O}_3$  Crystal by Ammonothermal Treatment: Reaction Pathways, Dynamics, and Chemical Stability. *J. Am. Chem. Soc.* **2014**, *136*, 11698–11706. [[CrossRef](#)]
35. Matsuishi, S.; Toda, Y.; Miyakawa, M.; Hayashi, K.; Kamiya, T.; Hirano, M.; Tanaka, I.; Hosono, H. High-Density Electron Anions in a Nanoporous Single Crystal:  $[\text{Ca}_{24}\text{Al}_{28}\text{O}_{64}]^{4+}(4\text{e}^-)$ . *Science* **2003**, *301*, 626–629. [[CrossRef](#)] [[PubMed](#)]
36. Kim, S.W.; Matsuishi, S.; Nomura, T.; Kubota, Y.; Takata, M.; Hayashi, K.; Kamiya, T.; Hirano, M.; Hosono, H. Metallic State in a Lime–Alumina Compound with Nanoporous Structure. *Nano Lett.* **2007**, *7*, 1138–1143. [[CrossRef](#)] [[PubMed](#)]
37. Kresse, G.; Furthmüller, J. Efficiency of ab-initio total energy calculations for metals and semiconductors using a plane-wave basis set. *Comput. Mater. Sci.* **1996**, *6*, 15–50. [[CrossRef](#)]
38. Kuganathan, N.; Green, J.C. Mercury telluride crystals encapsulated within single walled carbon nanotubes: A density functional study. *Int. J. Quantum Chem.* **2008**, *108*, 797–807. [[CrossRef](#)]
39. Kuganathan, N.; Green, J.C. 1D lead iodide crystals encapsulated within single walled carbon nanotubes. *Int. J. Quantum Chem.* **2009**, *109*, 171–175. [[CrossRef](#)]
40. Kuganathan, N.; Green, J.C. Crystal structure of low-dimensional Cu(I) iodide: DFT prediction of cuprophilic interactions. *Chem. Commun.* **2008**, 2432–2434. [[CrossRef](#)] [[PubMed](#)]
41. Kuganathan, N. Antimony Selenide Crystals Encapsulated within Single Walled Carbon Nanotubes—A DFT Study. *J. Chem.* **2009**, *6*, S147–S152. [[CrossRef](#)]
42. Calatayud, D.G.; Ge, H.; Kuganathan, N.; Mirabello, V.; Jacobs, R.M.J.; Rees, N.H.; Stoppiello, C.T.; Khlobystov, A.N.; Tyrrell, R.M.; Como, E.D.; Pascu, S.I. Encapsulation of Cadmium Selenide Nanocrystals in Biocompatible Nanotubes: DFT Calculations, X-ray Diffraction Investigations, and Confocal Fluorescence Imaging. *ChemistryOpen* **2018**, *7*, 144–158. [[CrossRef](#)]
43. Bichoutskaia, E.; Liu, Z.; Kuganathan, N.; Faulques, E.; Suenaga, K.; Shannon, I.J.; Sloan, J. High-precision imaging of an encapsulated Lindqvist ion and correlation of its structure and symmetry with quantum chemical calculations. *Nanoscale* **2012**, *4*, 1190–1199. [[CrossRef](#)]
44. Hu, Z.; Pantoş, G.D.; Kuganathan, N.; Arrowsmith, R.L.; Jacobs, R.M.J.; Kociok-Köhn, G.; O’Byrne, J.; Jurkschat, K.; Burgos, P.; Tyrrell, R.M.; Botchway, S.W.; Sanders, J.K.M.; Pascu, S.I. Interactions Between Amino Acid-Tagged Naphthalenediimide and Single Walled Carbon Nanotubes for the Design and Construction of New Bioimaging Probes. *Adv. Funct. Mater.* **2012**, *22*, 503–518. [[CrossRef](#)]
45. Mao, B.; Calatayud, D.G.; Mirabello, V.; Kuganathan, N.; Ge, H.; Jacobs, R.M.J.; Shepherd, A.M.; Ribeiro Martins, J.A.; Bernardino De La Serna, J.; Hodges, B.J.; Botchway, S.W.; Pascu, S.I. Fluorescence-Lifetime Imaging and Super-Resolution Microscopies Shed Light on the Directed- and Self-Assembly of Functional Porphyrins onto Carbon Nanotubes and Flat Surfaces. *Chem. A Eur. J.* **2017**, *23*, 9772–9789. [[CrossRef](#)] [[PubMed](#)]
46. Sloan, J.; Bichoutskaia, E.; Liu, Z.; Kuganathan, N.; Faulques, E.; Suenaga, K.; Shannon, I.J. Aberration corrected imaging of a carbon nanotube encapsulated Lindqvist Ion and correlation with Density Functional Theory. *J. Phys. Conf. Ser.* **2012**, *371*, 012018. [[CrossRef](#)]
47. Zoberbier, T.; Chamberlain, T.W.; Biskupek, J.; Kuganathan, N.; Eychusen, S.; Bichoutskaia, E.; Kaiser, U.; Khlobystov, A.N. Interactions and Reactions of Transition Metal Clusters with the Interior of Single-Walled Carbon Nanotubes Imaged at the Atomic Scale. *J. Am. Chem. Soc.* **2012**, *134*, 3073–3079. [[CrossRef](#)]
48. Kuganathan, N.; Chroneos, A. Encapsulation of cadmium telluride nanocrystals within single walled carbon nanotubes. *Inorg. Chim. Acta* **2019**, *488*, 246–254. [[CrossRef](#)]

49. Pascu, S.I.; Kuganathan, N.; Tong, L.H.; Jacobs, R.M.J.; Barnard, P.J.; Chu, B.T.; Huh, Y.; Tobias, G.; Salzmann, C.G.; Sanders, J.K.M.; Green, M.L.H.; Green, J.C. Interactions between tripodal porphyrin hosts and single walled carbon nanotubes: An experimental and theoretical (DFT) account. *J. Mater. Chem.* **2008**, *18*, 2781–2788. [[CrossRef](#)]
50. Chuvilin, A.; Bichoutskaia, E.; Gimenez-Lopez, M.C.; Chamberlain, T.W.; Rance, G.A.; Kuganathan, N.; Biskupek, J.; Kaiser, U.; Khlobystov, A.N. Self-assembly of a sulphur-terminated graphene nanoribbon within a single-walled carbon nanotube. *Nat. Mater.* **2011**, *10*, 687. [[CrossRef](#)]
51. Kuganathan, N. DFT Modelling of Tripeptides (Lysine-Tryptophan-Lysine) Interacting with Single Walled Carbon Nanotubes. *J. Chem.* **2010**, *7*, 870–874. [[CrossRef](#)]
52. Perdew, J.P.; Burke, K.; Ernzerhof, M. Generalized Gradient Approximation Made Simple. *Phys. Rev. Lett.* **1996**, *77*, 3865–3868. [[CrossRef](#)] [[PubMed](#)]
53. Monkhorst, H.J.; Pack, J.D. Special points for Brillouin-zone integrations. *Phys. Rev. B* **1976**, *13*, 5188–5192. [[CrossRef](#)]
54. Press, W.H.; Teukolsky, S.A.; Vetterling, W.T.; Flannery, B.P. *Numerical Recipes in C: The Art of Scientific Computing*, 2nd ed.; Cambridge University Press: Cambridge, UK, 1992; p. 994.
55. Grimme, S.; Antony, J.; Ehrlich, S.; Krieg, H. A consistent and accurate ab initio parametrization of density functional dispersion correction (DFT-D) for the 94 elements H-Pu. *J. Chem. Phys.* **2010**, *132*, 154104. [[CrossRef](#)]
56. Lam, D.J.; Darby, J.B.; Downey, J.W.; Norton, L.J.  $\alpha$ -Manganese Phases containing Technetium-99. *Nature* **1961**, *192*, 744. [[CrossRef](#)]
57. Henkelman, G.; Arnaldsson, A.; Jónsson, H. A fast and robust algorithm for Bader decomposition of charge density. *Comput. Mater. Sci.* **2006**, *36*, 354–360. [[CrossRef](#)]



© 2019 by the authors. Licensee MDPI, Basel, Switzerland. This article is an open access article distributed under the terms and conditions of the Creative Commons Attribution (CC BY) license (<http://creativecommons.org/licenses/by/4.0/>).